

Displaced cratonic mantle concentrates deep carbon during continental rifting

<https://doi.org/10.1038/s41586-020-2328-3>

Received: 19 August 2019

Accepted: 20 March 2020

Published online: 3 June 2020

 Check for updates

James D. Muirhead^{1,13}, Tobias P. Fischer², Sarah J. Oliva³, Amani Laizer⁴, Jolante van Wijk⁵, Claire A. Currie⁶, Hyunwoo Lee⁷, Emily J. Judd¹, Emmanuel Kazimoto⁴, Yuji Sano⁸, Naoto Takahata⁸, Christel Tiberi⁹, Stephen F. Foley¹⁰, Josef Dufek¹¹, Miriam C. Reiss¹² & Cynthia J. Ebinger³

Continental rifts are important sources of mantle carbon dioxide (CO₂) emission into Earth's atmosphere^{1–3}. Because deep carbon is stored for long periods in the lithospheric mantle^{4–6}, rift CO₂ flux depends on lithospheric processes that control melt and volatile transport^{1,3,7}. The influence of compositional and thickness differences between Archaean and Proterozoic lithosphere on deep-carbon fluxes remains untested. Here we propose that displacement of carbon-enriched Tanzanian cratonic mantle concentrates deep carbon below parts of the East African Rift System. Sources and fluxes of CO₂ and helium are examined over a 350-kilometre-long transect crossing the boundary between orogenic (Natron and Magadi basins) and cratonic (Balangida and Manyara basins) lithosphere from north to south. Areas of diffuse CO₂ degassing exhibit increasing mantle CO₂ flux and ³He/⁴He ratios as the rift transitions from Archaean (cratonic) to Proterozoic (orogenic) lithosphere. Active carbonatite magmatism also occurs near the craton edge. These data indicate that advection of the root of thick Archaean lithosphere laterally to the base of the much thinner adjacent Proterozoic lithosphere creates a zone of highly concentrated deep carbon. This mode of deep-carbon extraction may increase CO₂ fluxes in some continental rifts, helping to control the production and location of carbonate-rich magmas.

Abundant carbon is sequestered in mantle lithosphere during the infiltration of plume and carbon-rich silicate melts that are generated during mantle convection and periods of subduction^{5,6,8}, enriching mantle carbon contents by up to 100 times their original values⁶. Deep carbon accumulated by these processes is released during continental rifting^{8,9}. Rift-related CO₂ degassing thus has the potential to modulate Earth's climate on geological timescales¹²; however, the total volume of mantle CO₂ emitted at rift settings is poorly constrained, as are the deep lithospheric processes that control variations in mantle CO₂ flux.

The Eastern Rift of the East African Rift System (EARS; Fig. 1) is an ideal location to investigate the factors controlling rift CO₂ degassing, through measurements of active mantle CO₂ release^{1,10–12}. Given the large aerial extent, pervasive faulting and widespread magmatism in the EARS, quantifying the volume of CO₂ release requires observations from a wide variety of locations along the rift system. Results of diffuse soil degassing surveys have thus far been reported from the northern and central Main Ethiopian Rift⁷ and the Magadi and Natron basins¹, with estimated CO₂ fluxes of 0.52–4.36 Mt yr⁻¹ and 2.15–5.95 Mt yr⁻¹, respectively. Extrapolation of these estimates to the entire Eastern Rift

indicates potential CO₂ fluxes of the order of 10–100 Mt yr⁻¹. Current estimates of CO₂ degassing, however, do not consider spatial variations in mantle CO₂ release associated with diachronous rifting and variations in lithospheric thickness and composition.

The flux of CO₂ within any rift basin depends on a number of variables, such as the concentration of stored carbon in the lithosphere, the rates of melt production, the volume of the lithospheric mantle involved in melting and the available transport pathways^{6,7}. Geophysical data and numerical modelling show that lithospheric thinning, and the related magmatism, can occur in zones up to 10 times wider than the surface expression of a rift^{13,14}. Mantle convection and plume deflection near the base of the lithosphere will result in extensive lateral transport of hot mantle material that preferentially ponds and melts in zones of thinner lithosphere¹⁵. Lithosphere composition and structure also play a critical role in magma petrogenesis¹⁶. In the Eastern Rift, K/Na ratios increase from off- to on-craton localities, and carbonatite magmatism (Fig. 2) is spatially associated with potassium-enriched melts near the Tanzanian craton edge^{16–18}. Despite clear variations in the style and nature of magmatism in cratonic versus orogenic lithosphere, no

¹Department of Earth Sciences, Syracuse University, Syracuse, NY, USA. ²Department of Earth and Planetary Sciences, University of New Mexico, Albuquerque, NM, USA. ³Department of Earth and Environmental Sciences, Tulane University, New Orleans, LA, USA. ⁴Department of Geology, University of Dar es Salaam, Dar es Salaam, Tanzania. ⁵New Mexico Institute of Mining and Technology, Socorro, NM, USA. ⁶Department of Physics, University of Alberta, Edmonton, Alberta, Canada. ⁷School of Earth and Environmental Sciences, Seoul National University, Seoul, South Korea. ⁸Atmosphere and Ocean Research Institute, University of Tokyo, Chiba, Japan. ⁹Géosciences Montpellier, CNRS, Université de Montpellier, Montpellier, France. ¹⁰Department of Earth and Environmental Sciences, Macquarie University, North Ryde, New South Wales, Australia. ¹¹Department of Earth Sciences, University of Oregon, Eugene, OR, USA. ¹²Institute of Geosciences, Goethe University Frankfurt, Frankfurt am Main, Germany. ¹³Present address: School of Environment, University of Auckland, Auckland, New Zealand. ¹⁴e-mail: james.muirhead@fulbrightmail.org; fischer@unm.edu

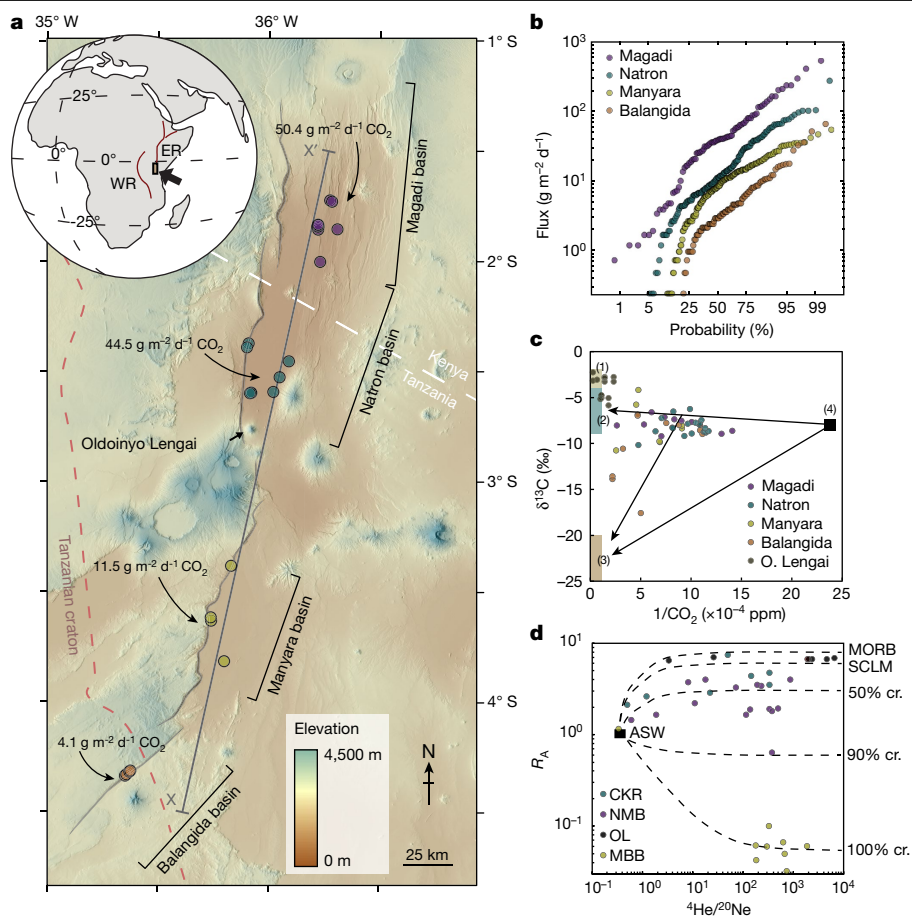


Fig. 1 | CO₂ flux and carbon and helium isotope data in the study region.

a, Annotated Shuttle Radar Topography Mission (SRTM) digital elevation model of the study region. Filled circles show the locations of the sampling regions, and CO₂ flux values represent mean values for high-flux populations in each basin (the helium isotope data in **d** support predominantly crustal volatile contributions in the Balangida and Manyara basins and mantle contribution in the Natron and Magadi basins). Border faults defining each basin are transparent grey. The dashed brown line delineates the surface expression of the eastward-dipping boundary for the Tanzanian craton. The cross-section line X–X' relates to the cross-sections presented in Fig. 3. The top left location inset also shows the Eastern Rift (ER) and Western Rift (WR) of the EARS.

study has so far examined how deep-carbon fluxes in the Eastern Rift vary across cratonic–orogenic boundaries, where gradients in the depth of the lithosphere–asthenosphere boundary can drive lateral advection of buoyant cratonic mantle into zones of lithospheric thinning¹⁹. We address this critical question by integrating recent and existing gas geochemical data with geophysical imaging of the EARS over an approximately 350-km-long transect extending southwards from orogenic to cratonic lithosphere^{20,21} (Fig. 1). By considering the results in the context of recent numerical models of the stability of cratonic lithosphere¹⁹, we propose a model of the lithosphere displacement of Tanzanian craton mantle that explains distinct variations observed in mantle CO₂ flux.

Rift degassing across a craton boundary

The Magadi, Natron, Manyara and Balangida basins (south Kenya and north Tanzania) form a series of kinematically linked rift segments representing an early expression (<7 million years ago; Ma) of continental rifting²² (Fig. 1a). These basins occur near the boundary between two major lithospheric terranes, the Archaean Tanzanian craton and Proterozoic Mozambique Belt of the Pan-African orogeny. The surface

b, Probability plots of diffuse CO₂ flux in each basin ($n = 547$). **c**, Carbon isotope content ($\delta^{13}\text{C}-\text{CO}_2$) versus the reciprocal of the CO₂ concentration⁴⁸ for diffuse CO₂ samples ($n = 62$). Shown are end-member carbon isotope values¹ for fumaroles (1), mantle (2), biogenic CO₂ (3) and air (4). **d**, $^3\text{He}/^4\text{He}$ data showing R_A versus $^4\text{He}/^{20}\text{Ne}$ for springs and fumaroles in the Eastern Rift of the EARS ($n = 38$), indicating mixing lines between air-saturated water (ASW) and endmembers (depleted mid-ocean ridge basalts, MORB, and sub-continental lithospheric mantle, SCLM) with varying proportions of crustal (cr.) helium. OL, Oldoinyo Lengai; CKR, Central Kenya Rift; NMB, Natron and Magadi basins; MBB, Manyara and Balangida basins. Analytical errors are discussed in Methods and do not exceed the size of the presented data points.

geological expression of the Tanzanian craton is observed only in the westernmost Balangida basin (Fig. 1a). However, xenolith data^{23–25} combined with geophysical constraints²¹ suggest that the Balangida and Manyara basins, and potentially parts of the southern Natron basin, lie predominantly above the Archaean Tanzanian craton¹⁶ rather than the Proterozoic lithosphere, which is present under the Natron and Magadi basins farther north. This interpretation is supported by the velocity and density structure of the lithosphere derived from a joint analysis of gravity and teleseismic data²¹, which reveals a distinct geophysical boundary with relatively low density and seismic velocities at depths of approximately 30–200 km below the Natron and Magadi basins (Fig. 3; see also Extended Data Fig. 1).

By investigating spring systems and areas of diffuse degassing situated along deeply penetrating faults of the Magadi, Natron, Manyara and Balangida basins, we examine how the nature of deep volatile transport varies across this craton boundary. Geophysical and gas geochemical data reveal the Natron and Magadi basins as key examples of active mantle CO₂ degassing^{1,20,26}, whereas mantle volatile discharges in the Manyara and Balangida basins are yet to be examined. Given the inherent variability of diffuse CO₂ flux within individual rift basins⁷, it is important to compare data from sites with similar structure, substrates

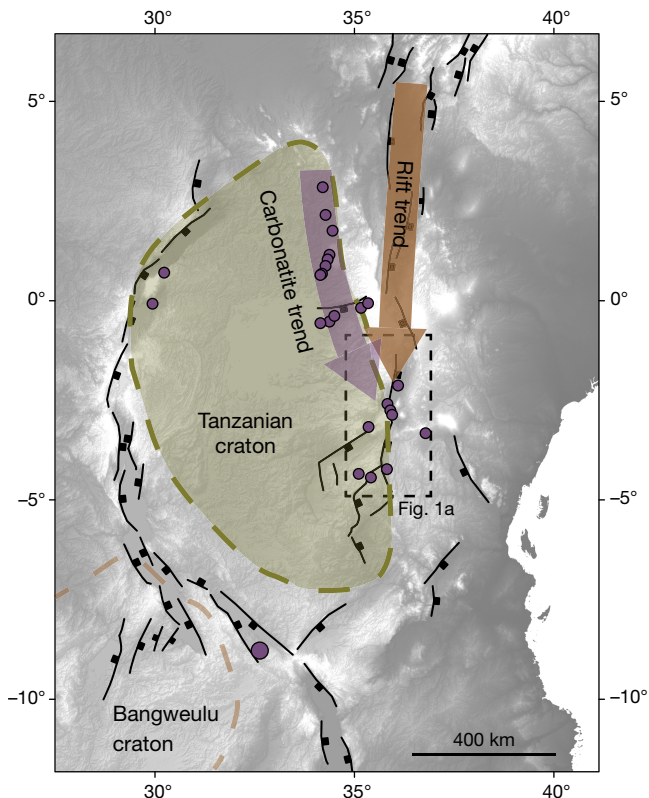


Fig. 2 | Distribution of <45-Myr-old carbonatite systems associated with the EARS and the Archaean Tanzanian craton. Carbonatites (purple circles) preferentially follow (purple arrow) the boundary of the Tanzanian craton (dashed line; craton boundary from Foley et al.¹⁶) rather than the dominant rift trend (brown arrow). The simplified distribution of major faults is presented as black solid lines. All features are annotated on the 90-m SRTM digital elevation model. The presented carbonatite systems are summarized in Supplementary Table 4.

and hydrology when comparing CO₂ discharges between basins. Therefore, we focus specifically on diffuse CO₂ flux data (1) from rift-graben sediments, (2) in the vicinity of faults and (3) in areas within 100 m of observed springs. Additionally, we present helium isotope data from springs, as well as diffuse gas flux and carbon and helium isotope data from Oldoinyo Lengai.

Volatile data exhibit a systematic north-to-south transition in the study region. Helium isotope data (³He/⁴He ratios) exhibit values ranging from 0.03R_A to 4.0R_A (R_A = ³He/⁴He ratio of air), with the highest values in the Natron and Magadi basins (0.7R_A–4.0R_A, average of (2.3 ± 1.1)R_A) compared to the Manyara ((0.05 ± 0.02)R_A) and Balangida ((0.05 ± 0.01)R_A) basins (Supplementary Table 3). These helium isotope ratios indicate that dissolved spring volatiles in the Manyara and Balangida basins have a crustal source (typically around 0.05R_A)²⁷. By contrast, ³He/⁴He ratios measured farther north in the Natron and Magadi basins reach up to 4.0R_A (ref.²⁷), approaching values almost as high as those inferred for the subcontinental lithospheric mantle (6.1R_A)²⁸. A subcontinental lithospheric mantle source for magma and volatiles in the Natron and Magadi basins is further supported by rare-earth and helium isotope data of lavas and xenoliths^{29,30}; by contrast, geochemical data^{30–33} suggest that plume melts are more prevalent in regions much farther north (for example, Ethiopia). Farther to the south, that is, in the Rungwe Volcanic Province, some helium isotope data of xenoliths suggest plume melt sources³⁴, whereas radiogenic isotopes display characteristics inconsistent with primitive mafic lavas of the Afar Depression, Ethiopia³⁰.

Carbon isotope data of diffusely degassing CO₂ (δ¹³C-CO₂; see Methods) indicate predominantly mantle carbon sources in the Natron and

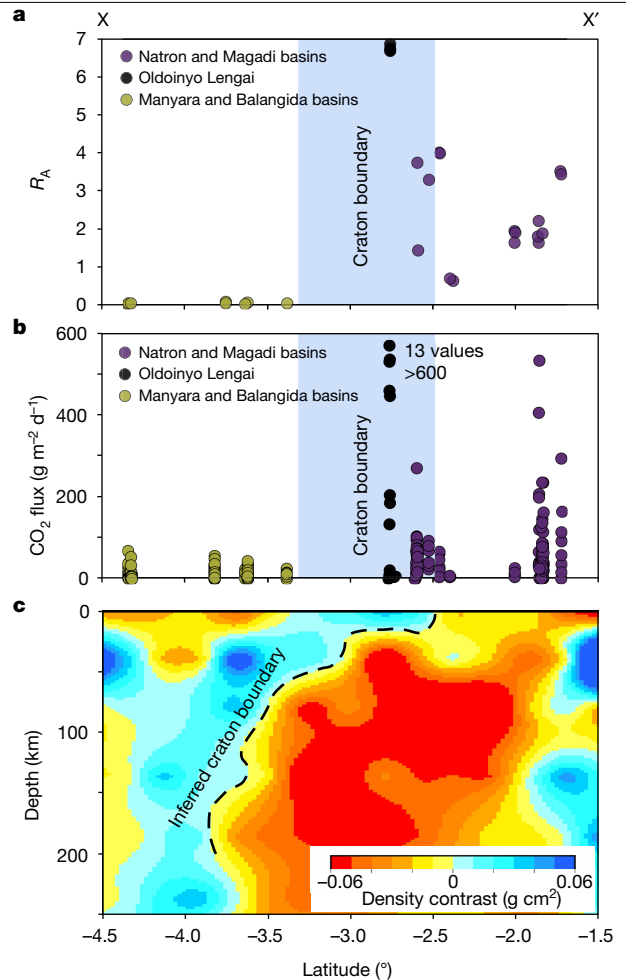


Fig. 3 | Latitudinal variations in CO₂ flux and R_A values for ³He/⁴He with respect to the modelled lithosphere structure. **a**, R_A versus latitude along the Eastern Rift from –1.5° to –4.5° (n = 25). Air-contaminated samples (TZ18-C16) were removed from the analysis. The Tanzanian craton boundary (light grey) is interpreted on the basis of sharp density (c) and velocity contrasts near the northern Manyara and southern Natron basins (see also Extended Data Fig. 1). It is marked as a broad region to account for location uncertainties and the overall three-dimensional nature of the boundary in the region (see also Methods). **b**, Diffuse CO₂ flux versus latitude along the Eastern Rift from –1.5° to –4.5° for the sample sites presented in Fig. 1a and Oldoinyo Lengai volcano (n = 610). **c**, Lithosphere density model from Tiberi et al.²¹. Contrasts are relative to the IASP91 model⁴⁹. The position of the cross-section is shown in Fig. 1a.

Magadi basins^{1,27}, with progressively more mixing between biogenic and perhaps crustal CO₂ southwards into the Manyara and Balangida basins (Fig. 1). Additionally, we observe a north-to-south decrease in the flux of diffusely degassing CO₂ (Figs. 1, 3), where mean values for the high-CO₂-flux populations in the Natron and Magadi basins drop from 44.5–50.4 g m^{–2} d^{–1} to 4.1–11.5 g m^{–2} d^{–1} in the Balangida and Manyara basins (Extended Data Fig. 2). This comparison also does not consider substantial degassing from the Oldoinyo Lengai volcano in the Natron basin¹⁰, which exhibits the highest diffuse CO₂ flux measurements in the region (up to 7,376 g m^{–2} d^{–1}), suggesting that the Natron basin is probably the major carbon emitter in this sector of the EARS (Fig. 3). The Balangida and Manyara basins exhibit a considerably lower overall CO₂ flux, and ³He/⁴He ratios (0.03R_A to 0.07R_A) support the release of predominantly crustal volatiles. These two observations suggest that the lower diffuse CO₂ fluxes here probably represent a mixed biogenic and minor crustal carbon source, such as that released by dissolution of limestone²⁷. In summary, data collected in the Manyara and Balangida

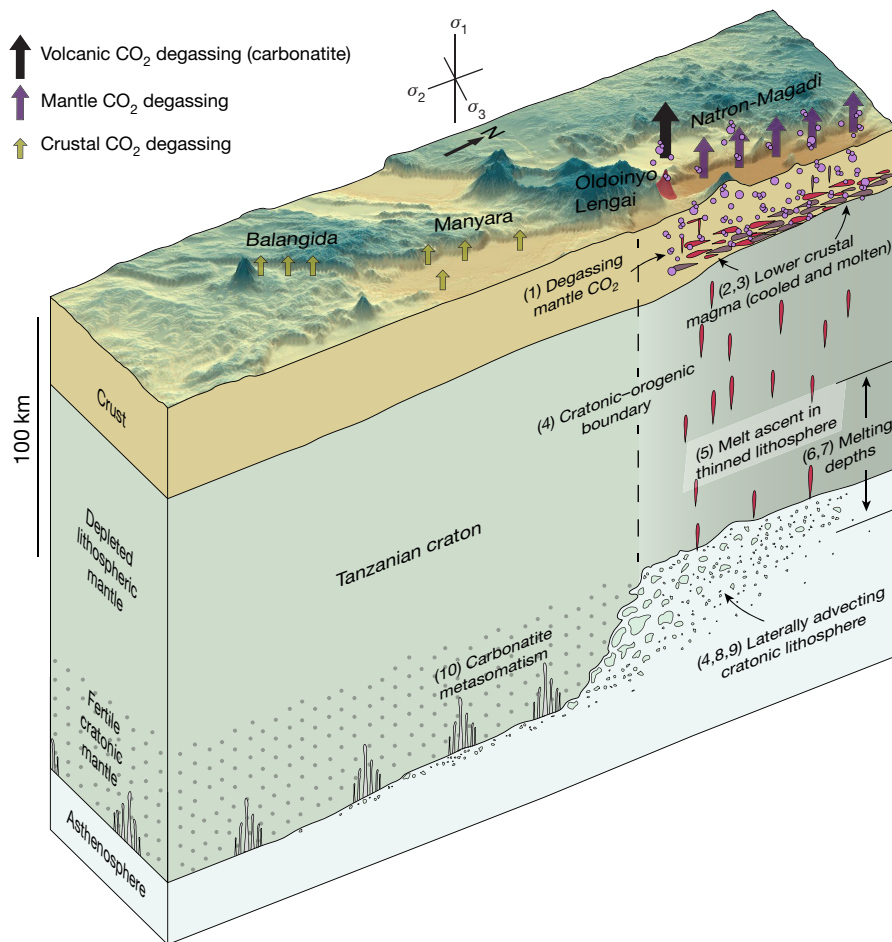


Fig. 4 | Proposed model for deep-carbon transport along a cratonic boundary in the EARS study region. Cratonic mantle lithosphere is advected laterally and vertically into a region of melting near the cratonic boundary. CO_2 -rich melts rise through the thinning mobile belt, intrude the lower crust and degas, or erupt at the surface as highly alkaline or carbonatite lavas. The

tectonic stress state is represented as the highest (σ_1), intermediate (σ_2) and lowest (σ_3) compressive stresses. Data from (1) Lee et al.¹; (2) Roecker et al.²⁰; (3) Ebinger et al.²²; (4) Tiberi et al.²¹; (5) Selway³⁵; (6) Mana et al.²⁹; (7) Dawson et al.⁵⁰; (8) Currie & van Wijk¹⁹; (9) Huismans and Beaumont³⁹; (10) Rudnick et al.³⁸.

basins clearly show that there is negligible mantle volatile degassing locally through the Archaean Tanzania craton. Furthermore, helium data indicate predominantly crustal volatile discharges and, combined with the low CO_2 fluxes, suggest that the craton here is either not a substantial source of mantle carbon and/or represents an impermeable barrier to the ascent of mantle carbon³⁵. Given the probable accumulation of carbon in the lower cratonic lithosphere over time^{6,9}, the latter explanation is more likely.

Lithospheric transport of cratonic carbon

Continental rifts are rife with dilational fault systems that act as permeable conduits for the ascent of deep mantle volatiles released from cooling magmas^{1,3}, which are extracted from volatile-rich, sub-continental lithospheric mantle⁶. Reconstructions of continental rift lengths over the last 200 million years suggest a potential positive correlation between rift length and partial pressure of atmospheric CO_2 (ref. ²). However, estimates of CO_2 fluxes from continental rift settings in Earth's geological past are informed by present-day measurements, with the EARS being a typical example of voluminous rift degassing^{1,7}. Calculated global fluxes of CO_2 from continental rifts² thus consider mean fluxes from relatively sparse measurements^{1,7}, neglecting process-driven spatial variations in mantle carbon release both in the present and in the geological past. Indeed, our results indicate dramatic spatial variations in mantle CO_2 flux between adjacent rift

basins in the Eastern Rift and associations with carbonate-rich melt generation near craton–orogen boundaries (Figs. 1–3). It is therefore likely that there are deep processes at play that act to concentrate mantle carbon below specific rift sectors, driving these observed CO_2 flux variations.

Which processes promote higher fluxes and concentrations of mantle CO_2 in a continental rift? One potential answer could be that the cratonic mantle lithosphere is carbon-poor compared to neighbouring lithospheric terranes. However, given the age of the Archaean terrane, it is expected that there are deep-carbon stores in the lowermost lithospheric mantle from infiltration related to previous plume magmatism, mantle convection and subduction–collision that occurred over approximately the past 3 Gyr (refs. ^{6,36}). Geophysical and petrological data indicate that the Archaean lithosphere is hydrated relative to the neighbouring Proterozoic lithosphere^{24,33,36}, in part from a kimberlite intrusion phase during initial plume impingement. The 53–40-Myr-old Mwadui kimberlites in the eastern Tanzanian craton contain inclusions in diamonds that attest to the presence of mantle metasomatism around 10–25 Myr before EARS rifting³⁷; these include a high concentration of TiO_2 in garnets and K_2O in clinopyroxene, as well as a high ratio of lherzolitic to harzburgitic inclusions, indicating re-fertilization of the cratonic lithosphere at depths of >180 km. In northern Tanzania (Fig. 1a), trace element relationships of spinel peridotite xenoliths enriched in light rare-earth elements support mantle metasomatism through addition of carbonatite melts³⁸.

Given the fertile and carbon-enriched lithospheric mantle in the eastern Tanzanian craton, the negligible CO₂ fluxes and crustal ³He/⁴He ratios in the Manyara and Balangida basins could represent purely lower rates of magma production. However, comparison of geochemical data with existing geophysical results²¹ suggests a potentially deep (>200 km) lithospheric control on melt and CO₂ transport in this section of the EARS. The modelled seismic velocity and density increase rapidly southwards of the Natron basin (Fig. 3), and the velocity changes coincide with the suture between the Tanzanian craton and Proterozoic Mozambique Belt²¹. Numerical models of buoyant and relatively hydrated cratonic mantle, such as the Tanzanian craton^{24,35,38}, predict that edge convection does not develop at such a craton boundary¹⁹. Instead, the weak cratonic material is laterally advected for distances of up to 125 km towards mobile belts and then transported upwards near craton–mobile belt boundaries^{19,39}. Mantle xenolith analyses provide evidence for thinning of the Tanzanian craton and the presence of Archaean lithosphere below the Natron Basin⁴⁰. This mechanical dislodgment of deep-carbon-rich lithosphere increases the probability of carbonate melt production, through entrainment in warmer asthenosphere and related decompression as the material rises to the base of the mobile belt. If very low degrees of melting occur near the base of the craton at depths of around 200 km in even mildly oxidizing conditions, then melts will be strongly enriched in carbonate⁴¹. However, it is uncertain whether lateral migration of melts is efficient enough to concentrate so much carbon beneath the Magadi and Natron basins in the comparatively carbon-poor Proterozoic lithosphere. As such, we propose that displaced, carbon-enriched cratonic mantle lithosphere is present below the Magadi and Natron basins. This model best explains the high CO₂ flux and the cause of carbon-rich melt production at this location, and is favoured over edge-driven convection, which is suppressed in the presence of metasomatized cratonic mantle¹⁹.

In this model (Fig. 4), stores of fertile lithospheric mantle are removed from the base of the Archaean craton and transported laterally (guided by the slow northeast movement of Africa in a no-net rotation reference frame⁴²). They also rise upwards into thinned lithosphere in the Natron and Magadi basins to drive melting of carbon-rich mantle. These deeper sections of cratonic mantle contain abundant diamonds trapped by redox freezing or carbonate in dykes of phlogopite pyroxenite⁹, which melt preferentially during upward movement, explaining the association of carbonate with potassium-rich magmatism. The sheared and thinned Proterozoic lithosphere then serves to focus and enhance melt and volatile migration through the plate^{15,35}. Additionally, the zone of melting below the rift along the craton edge is consistently replenished in carbon from the lateral migration of fertile Archaean lithosphere (Fig. 4). This effect results in greater mantle CO₂ and melt fluxes at the surface in the Natron and Magadi basins. Active carbonatite magmatism occurs near this rheologic boundary (Fig. 2), where volatile sources abruptly transition south to north from the crust to the mantle. Our proposed model therefore explains why the Natron and Magadi basins represents the region of highest estimated tectonic degassing of mantle CO₂ in the EARS¹ (2.15–5.95 Mt yr⁻¹) and has remained a region of persistent carbon-rich magmatism for approximately the past 4 Myr (for example, carbonatite volcanism at the Mosonik, Satiman, Shompole, Kerimasi and then Oldoinyo Lengai volcanoes; Fig. 2, Supplementary Table 4) and why some carbonatite melts are generated below the comparatively carbon-poor orogenic lithosphere near the craton border (for example, the Shompole volcano; Supplementary Table 4).

The mode of deep-carbon extraction and transport presented here has implications for constraining global outputs of CO₂ from extensional tectonic settings and the generation of carbon-rich magmas. Rare occurrences of carbonatite magmatism, such as that observed at Oldoinyo Lengai, do not depend exclusively on anomalously carbon-enriched mantle sources⁴³, but may manifest owing to lithospheric conditions that allow the focusing of deep carbon. Occurrences of within-rift carbonatite volcanoes in northern Tanzania are

restricted to zones where the EARS intersects the thick Tanzanian craton (Fig. 2). Further north in Kenya and Uganda, carbonatite volcanism has manifested off-axis and continues to follow the north-northwest trending boundary of the Archaean Tanzanian and Kibalian cratons¹⁷, rather than the EARS, which trends north-northeast to south-southwest in the Kenyan and Main Ethiopian rifts. On the western side of the craton, similar trends are observed: large quantities of SO₂ (ref. ⁴⁴) and CO₂ are emitted from Nyamuragira⁴⁵; recent carbonatite volcanism at Katwe-Kikorongo and the Fort Portal volcanic field; and Miocene carbonatites in Rukwa between the Tanzanian and Bangweulu cratons^{16,46,47} (Fig. 2; Supplementary Table 4). Together, these observations are consistent with the hypothesis that mantle carbon is transported towards, and concentrated along, the edges of Archaean cratons, where melt more efficiently ascends upwards along pressure gradients beneath thinner lithosphere through extending and more permeable lithosphere⁹. From here, crustal-scale, permeable faults¹ and carbonatite volcanism¹⁰ facilitate release of sizable carbon stores in regions such as the Natron and Magadi basins.

Our proposed model of advective removal of fertile cratonic lithosphere (Fig. 4) can increase and sustain CO₂ fluxes in continental rifts situated adjacent to cratonic edges. This implies that global estimates of mantle CO₂ flux from continental rifts must account for both across- and along-strike variations in lithospheric thickness, composition and rheology in these systems.

Online content

Any methods, additional references, Nature Research reporting summaries, source data, extended data, supplementary information, acknowledgements, peer review information; details of author contributions and competing interests; and statements of data and code availability are available at <https://doi.org/10.1038/s41586-020-2328-3>.

- Lee, H. et al. Massive and prolonged deep carbon emissions associated with continental rifting. *Nat. Geosci.* **9**, 145–149 (2016).
- Brune, S., Williams, S. E. & Müller, R. D. Potential links between continental rifting, CO₂ degassing and climate change through time. *Nat. Geosci.* **10**, 941–946 (2017).
- Tamburello, G., Pondrelli, S., Chiodini, G. & Rouwet, D. Global-scale control of extensional tectonics on CO₂ earth degassing. *Nat. Commun.* **9**, 4608 (2018).
- Dasgupta, R. & Hirschmann, M. M. The deep carbon cycle and melting in Earth's interior. *Earth Planet. Sci. Lett.* **298**, 1–13 (2010).
- Kelemen, P. B. & Manning, C. E. Reevaluating carbon fluxes in subduction zones, what goes down, mostly comes up. *Proc. Natl Acad. Sci. USA* **112**, E3997–E4006 (2015).
- Foley, S. F. & Fischer, T. P. An essential role for continental rifts and lithosphere in the deep carbon cycle. *Nat. Geosci.* **10**, 897–902 (2017).
- Hunt, J. A., Zafu, A., Mather, T. A., Pyle, D. M. & Barry, P. H. Spatially variable CO₂ degassing in the main Ethiopian rift: implications for magma storage, volatile transport, and rift-related emissions. *Geochem. Geophys. Geosyst.* **18**, 3714–3737 (2017).
- Malusà, M. G. et al. Active carbon sequestration in the Alpine mantle wedge and implications for long-term climate trends. *Sci. Rep.* **8**, 4740–4748 (2018).
- Foley, S. F. Rejuvenation and erosion of the cratonic lithosphere. *Nat. Geosci.* **1**, 503–510 (2008).
- Brantley, S. L. & Koepnick, K. W. Measured carbon-dioxide emissions from Oldoinyo Lengai and the skewed distribution of passive volcanic fluxes. *Geology* **23**, 933–936 (1995).
- Sawyer, G. M., Carn, S. A., Tsanev, V. I., Oppenheimer, C. & Burton, M. Investigation into magma degassing at Nyiragongo volcano, Democratic Republic of the Congo. *Geochem. Geophys. Geosyst.* **9**, Q02017 (2008).
- Hutchison, W. et al. Structural controls on fluid pathways in an active rift system: a case study of the Aluto volcanic complex. *Geosphere* **11**, 542–562 (2015).
- van Wijk, J., van Hunen, J. & Goes, S. Small-scale convection during continental rifting: evidence from the Rio Grande rift. *Geology* **36**, 575–578 (2008).
- Bastow, I. D., Keir, D. & Daly, E. The Ethiopia Afar Geoscientific Lithospheric Experiment (EAGLE): probing the transition from continental rifting to incipient seafloor spreading. *Spec. Pap. Geol. Soc. Am.* **478**, 1–26 (2011).
- Ebinger, C. J. & Sleep, N. H. Cenozoic magmatism throughout east Africa resulting from impact of a single plume. *Nature* **395**, 788–791 (1998).
- Foley, S. F., Link, K., Tiberindwa, J. V. & Barifaijo, E. Patterns and origin of igneous activity around the Tanzanian craton. *J. Afr. Earth Sci.* **62**, 1–18 (2012).
- Kalt, A., Hegner, E. & Satir, M. Nd, Sr, and Pb isotopic evidence for diverse lithospheric mantle sources of East African Rift carbonatites. *Tectonophysics* **278**, 31–45 (1997).
- Rosenthal, A., Foley, S. F., Pearson, D. G., Nowell, G. M. & Tappe, S. Petrogenesis of strongly alkaline primitive volcanic rocks at the propagating tip of the western branch of the East African Rift. *Earth Planet. Sci. Lett.* **284**, 236–248 (2009).
- Currie, C. A. & van Wijk, J. How craton margins are preserved: insights from geodynamic models. *J. Geodyn.* **100**, 144–158 (2016).

20. Roecker, S. et al. Subsurface images of the Eastern Rift, Africa, from the joint inversion of body waves, surface waves and gravity: investigating the role of fluids in early-stage continental rifting. *Geophys. J. Int.* **210**, 931–950 (2017).
21. Tiberi, C. et al. Lithospheric modification by extension and magmatism at the craton–orogenic boundary: north Tanzania divergence, East Africa. *Geophys. J. Int.* **216**, 1693–1710 (2019).
22. Ebinger, C. J. et al. Crustal structure of active deformation zones in Africa: implications for global crustal processes. *Tectonics* **36**, 3298–3332 (2017).
23. Lee, C. T. & Rudnick, R. L. Compositionally stratified cratonic lithosphere: petrology and geochemistry of peridotite xenoliths from the Labait tuff cone, Tanzania. In *Proc. of the 7th International Kimberlite Conference* (eds Gurney, J. J. & Richardson, S. R.) 503–309 (National Book Printers, 1999).
24. Vauchez, A., Dineur, F. & Rudnick, R. Microstructure, texture and seismic anisotropy of the lithospheric mantle above a mantle plume: insights from the Labait volcano xenoliths (Tanzania). *Earth Planet. Sci. Lett.* **232**, 295–314 (2005).
25. Aulbach, S., Rudnick, R. L. & McDonough, W. F. Evolution of the lithospheric mantle beneath the East African Rift in Tanzania and its potential signatures in rift magmas. *Spec. Pap. Geol. Soc. Am.* **478**, 105–125 (2011).
26. Weinstein, A. et al. Fault–magma interactions during early continental rifting: seismicity of the Magadi–Natron–Manyara basins, Africa. *Geochem. Geophys. Geosyst.* **18**, 3662–3686 (2017).
27. Lee, H. et al. Incipient rifting accompanied by the release of subcontinental lithospheric mantle volatiles in the Magadi and Natron basin, East Africa. *J. Volcanol. Geotherm. Res.* **346**, 118–133 (2017).
28. Gautheron, C. & Moreira, M. Helium signature of the subcontinental lithospheric mantle. *Earth Planet. Sci. Lett.* **199**, 39–47 (2002).
29. Mana, S., Furman, T., Turrin, B. D., Feigenson, M. D. & Swisher, C. C. Magmatic activity across the East African North Tanzanian Divergence Zone. *J. Geol. Soc. Lond.* **172**, 368–389 (2015).
30. Halldórsson, S. A., Hilton, D. R., Scarsi, P., Abebe, T. & Hopp, J. A common mantle plume source beneath the entire East African Rift System revealed by coupled helium–neon systematics. *Geophys. Res. Lett.* **41**, 2304–2311 (2014).
31. Furman, T. et al. Heads and tails: 30 million years of the Afar plume. *Geol. Soc. Lond. Spec. Publ.* **259**, 95–119 (2006).
32. Furman, T. Geochemistry of East African Rift basalts: an overview. *J. Afr. Earth Sci.* **48**, 147–160 (2007).
33. Pik, R., Marty, B. & Hilton, D. R. How many mantle plumes in Africa? The geochemical point of view. *Chem. Geol.* **226**, 100–114 (2006).
34. Hilton, D. R. et al. Helium isotopes at Rungwe Volcanic Province, Tanzania, and the origin of East African Plateaux. *Geophys. Res. Lett.* **38**, L21304 (2011).
35. Selway, K. Negligible effect of hydrogen content on plate strength in East Africa. *Nat. Geosci.* **8**, 543–546 (2015).
36. Koorneef, J. M. et al. Nature and timing of multiple metasomatic events in the sub-cratonic lithosphere beneath Labait, Tanzania. *Lithos* **112**, 896–912 (2009).
37. Stachel, T. & Brey, G. P. Rare and unusual mineral inclusions in diamonds from Mwadui, Tanzania. *Contrib. Mineral. Petrol.* **132**, 34–47 (1998).
38. Rudnick, R. L., McDonough, W. F. & Chappell, B. W. Carbonatite metasomatism in the northern Tanzanian mantle: petrographic and geochemical characteristics. *Earth Planet. Sci. Lett.* **114**, 463–475 (1993).
39. Huismans, R. & Beaumont, C. Depth-dependent extension, two-stage breakup and cratonic underplating at rifted margins. *Nature* **473**, 74–78 (2011).
40. Chesley, J. T., Rudnick, R. L. & Lee, C.-T. Re–Os systematics of mantle xenoliths from the East African Rift: age, structure, and history of the Tanzanian craton. *Geochim. Cosmochim. Acta* **63**, 1203–1217 (1999).
41. Foley, S. F. et al. The composition of near-solidus melts of peridotite in the presence of CO₂ and H₂O between 40 and 60 kbar. *Lithos* **112**, 274–283 (2009).
42. Conrad, C. P. & Behn, M. D. Constraints on lithosphere net rotation and asthenospheric viscosity from global mantle flow models and seismic anisotropy. *Geochem. Geophys. Geosyst.* **11**, Q05W05 (2010).
43. Fischer, T. P. et al. Upper-mantle volatile chemistry at Oldoinyo Lengai volcano and the origin of carbonatites. *Nature* **459**, 77–80 (2009).
44. Carn, S. A., Fioletov, V. E., McLinden, C. A., Li, C. & Krotkov, N. A. A decade of global volcanic SO₂ emissions measured from space. *Sci. Rep.* **7**, 44095 (2017).
45. Sawyer, G. M., Carn, S. A., Tsanev, V. I., Oppenheimer, C. & Burton, M. Investigation into magma degassing at Nyiragongo volcano, Democratic Republic of the Congo. *Geochem. Geophys. Geosyst.* **9**, Q02017 (2008).
46. Eby, G. N., Lloyd, F. E. & Woolley, A. R. Geochemistry and petrogenesis of the Fort Portal, Uganda, extrusive carbonatite. *Lithos* **113**, 785–800 (2009).
47. Roberts, E. M. et al. Initiation of the western branch of the East African Rift coeval with the eastern branch. *Nat. Geosci.* **5**, 289–294 (2012).
48. Parks, M. M. et al. Distinguishing contributions to diffuse CO₂ emissions in volcanic areas from magmatic degassing and thermal decarbonation using soil gas ²²²Rn–^δ¹³C systematics: application to Santorini volcano, Greece. *Earth Planet. Sci. Lett.* **377**, 180–190 (2013).
49. Kennett, B. L. N. & Engdahl, E. R. Traveltimes for global earthquake location and phase identification. *Geophys. J. Int.* **105**, 429–465 (1991).
50. Dawson, J. B., James, D., Paslick, C. & Halliday, A. M. Ultrabasic potassic low-volume magmatism and continental rifting in north-central Tanzania: association with enhanced heat flow. *Russ. Geol. Geophys.* **38**, 69–81 (1997).

Publisher's note Springer Nature remains neutral with regard to jurisdictional claims in published maps and institutional affiliations.

© The Author(s), under exclusive licence to Springer Nature Limited 2020

Methods

We use existing CO₂ flux, helium isotope and carbon isotope data from the Central Kenya Rift and the Natron, Magadi and Manyara basins, and recent data collected in the Natron, Manyara and Balangida basins (Supplementary Data Tables 1–3). To better interpret these data within the context of existing models of mantle volatile transport, we compare our results with a geophysically defined cratonic boundary from Tiberi et al.²¹ and the distribution of carbonatite volcanoes, discussed below.

Defining the craton boundary and uncertainty in the seismic velocity model

The boundary of the Tanzanian craton in the study region is broadly defined using the seismic velocity and density structure of the lithosphere derived from a joint analysis of gravity and teleseismic data from Tiberi et al.²¹, which shows a sharp velocity gradient, perhaps due to the presence of displaced low-density lower cratonic mantle and/or the presence of melt and other fluids^{20,21,26}. The boundary in Fig. 3 (also shown in Extended Data Fig. 1) is presented as a broad zone to account for the complex three-dimensional nature of the boundary (compared to the two-dimensional cross-section line shown) and the uncertainty in the model resolution. A slightly modified version of Fig. 3 is presented here to facilitate comparison of the possible location of the craton boundary from the seismic velocity model (Extended Data Fig. 1). Teleseismic tomography suffers from a lack of vertical resolution, particularly within the upper 30 km. However, its lateral resolution is high and mostly depends on the station interspacing. Synthetic tests show that an interstation length of ~20 km enables resolution of lateral boundaries to 15 km in the upper 100 km of the velocity model (see supplementary materials in Tiberi et al.²¹). Moreover, the authors combine seismic delay times with gravity data in the inversion scheme, which increases crustal resolution. Higher resolution crustal imaging at depths of <40 km can be found in Roecker et al.²⁰ and Ibs-von Seht et al.⁵¹. Crustal structures as narrow as 6 km can be resolved in the joint inversion of arrival times, ambient noise and gravity in Roecker et al.²⁰.

Areas of carbonatite volcanism associated with the EARS

We set an age threshold of 45 Myr for carbonatite volcanism associated with the development of the EARS, which is consistent with Ernst & Bell⁵². Although the age and initiation of the EARS is often linked with the eruption of Oligocene trap lavas between ~33.9 Ma and 27 Ma (refs. ^{32,53,54}), 45–34-Myr-old flood lavas are identified in the Turkana region (North Kenya) and the Southern Ethiopian plateau with geochemical affinities to 33.9–22-Myr-old EARS lavas, suggesting a potentially longer-lived thermo-chemical anomaly associated with EARS rifting^{32,54}.

Supplementary Data Table 4 provides a summary of the location and age of <45-Myr-old carbonatite centres associated with the EARS^{29,47,52,55–62}. A few of these volcanoes in Uganda have no reported ages, but form part of a sub-linear belt of carbonatite volcanoes, all with reported ages <45 Myr. Therefore, we considered these carbonatite systems to be associated with magmatism and rifting in the EARS, consistent with the interpretation of Ernst & Bell⁵² for these carbonatites. Additionally, the exact location of <45-Myr-old carbonatite volcanoes in the Rukwa/Rungwe region are tentatively assigned, because they are identified only through observations of distal carbonatite tephra deposits⁴⁷, with only Mesozoic ages assigned to mapped carbonatite volcanoes.

Model of active mantle volatile degassing in the Natron and Magadi basins

Previous geochemical and geophysical studies investigating active seismicity and volatile discharge in the Natron and Magadi basins support mantle volatile transport through fault and fracture networks,

which is further corroborated by recent helium and carbon isotope data presented in this study. Recent seismic station deployments (for example, the CRAFTI network²⁶) have detected persistent low-magnitude earthquakes since 2013 that span the full range of the crust. Abundant seismic activity occurs at mid- to lower-crustal depths (for example, 15–40 km), where P- and S-wave velocities (V_p and V_s , respectively) suggest the presence of discrete magma chambers at various depths. Lower-crustal earthquakes occur in regions of low V_p/V_s , indicating the presence of compressible pore fluids²⁰, and correspond to deeply penetrating border faults that actively emit mantle volatiles^{1,27}. Collectively, these data support the presence of deep crustal magma bodies in the Natron and Magadi basins, which are probably generated from a sub-continental lithospheric melt source^{27,29} that actively releases mantle volatiles into the overlying extensional fault system^{1,26,58}. On the basis of these observations, a tectonic degassing model⁶³ has been proposed for the Natron and Magadi basin¹, where mantle volatiles (including CO₂) escape along fault and fracture networks at the surface and in regions not directly affected by volcanism.

Laboratory analyses of thermal springs

Thermal-spring samples were collected in copper tubes and analysed for ³He/⁴He ratios on noble gas mass spectrometers (Helix-SFT and VG-5400) at the Atmosphere and Ocean Research Institute of the University of Tokyo (AORI). Both He and Ne were purified using hot titanium getters (at 400 °C) and charcoal traps (at liquid-nitrogen temperature), and Ne was removed using a cryogenic trap (at 40 K) after measuring ⁴He/²⁰Ne ratios using a quadrupole mass spectrometer (Prisma 80 QMS, Pfeiffer). The experimental errors for ³He/⁴He and ⁴He/²⁰Ne ratios are about 1% and 5% (1 σ ; SFT-Helix) and about 3.5% and 5% (1 σ ; VG5400), respectively⁶⁴.

Flux measurement and analyses of carbon isotopes of diffuse CO₂

The flux of diffusely degassing CO₂ in each study location was measured using EGM-4 and EGM-5 gas analysers (PP Systems), which have a measurement range of 0–30,000 ppm and <1% error. For each measurement, a cylindrical chamber with a volume of 1.18×10^{-3} m³ was placed on the ground forming a tight seal, and the CO₂ flux was calculated using changes in CO₂ concentration over a 120-s timespan. Diffuse gas samples were also collected by diverting gas from the chamber into pre-evacuated glass vials, and CO₂ concentrations were recorded at the time of sampling. Gas samples were analysed using a Finnigan Delta XL Isotope Ratio Mass Spectrometer with a gas bench and auto-sampler at the Center for Stable Isotopes, University of New Mexico. Measured values are reported relative to the Vienna Pee Dee belemnite (VPDB) standard and presented as $\delta^{13}\text{C}$ values in parts per thousand (‰) in Fig. 1. Fractionation effects between ionized carbon (HCO₃⁻ and CO₃²⁻) and CO₂ gases in the Natron and Magadi basin hydrothermal systems were examined by Lee et al.²⁷, who found corrected $\delta^{13}\text{C}$ values ranging from -0‰ to -7‰. These values are consistent with predominantly mantle-derived carbon and are within the range of soil gas samples collected in Natron and Magadi for this study, which range from -2.2‰ to 10.1‰.

Differentiating CO₂ flux populations

Discrimination of different sources of diffusely degassing CO₂ in volcano-tectonic settings is often achieved through a combination of carbon isotope analyses and statistical analyses of CO₂ flux populations^{1,65,66}. This process differentiates two or more CO₂ flux populations exhibiting log-normal distributions, with the highest mean flux often attributed to a magmatic population¹⁰, which can be corroborated through isotopic analyses⁶⁶. To make these subdivisions, we use the method of Sinclair⁶⁷ adopted in Chiodini et al.⁶⁵, where flux populations are delineated on either side of a distinct inflection point on logarithmic probability plots (Extended Data Fig. 2).

Data availability

All data generated or analysed during this study are provided with this article and in Supplementary Tables 1–4. The SRTM digital elevation model used to generate maps is publicly available at <http://srtm.csi.cgiar.org/srtmdata>. The recently analysed and previously unpublished CO₂ flux and isotopic data (<https://doi.org/10.26022/IEDA/111520>) from the 2018 Tanzania field campaign can be found at <http://www.earthchem.org>.

51. Ibs-von Seht, M., Blumenstein, S., Wagner, R., Hollnack, D. & Wohlenberg, J. Seismicity, seismotectonics and crustal structure of the southern Kenya Rift—new data from the Lake Magadi area. *Geophys. J. Int.* **146**, 439–453 (2001).
52. Ernst, R. E. & Bell, K. Large igneous provinces (LIPs) and carbonatites. *Mineral. Petrol.* **98**, 55–76 (2010).
53. Hofmann, C. et al. Timing of the Ethiopian flood basalt event and implications for plume birth and global change. *Nature* **389**, 838–841 (1997).
54. Rooney, T. O. The Cenozoic magmatism of East-Africa: Part I – flood basalts and pulsed magmatism. *Lithos* **286–287**, 264–301 (2017).
55. Woolley, A. R. & Kjarvsgaard, B. A. *Carbonatite Occurrences of the World* (Geological Survey of Canada, 2008).
56. Fairhead, J. D., Mitchell, J. G. & Williams, L. A. J. New K/Ar determinations on rift volcanics of S. Kenya and their bearing on age of rift faulting. *Science* **238**, 66–69 (1972).
57. Le Gall, B. et al. Rift propagation at craton margin. Distribution of faulting and volcanism in the North Tanzanian Divergence (East Africa) during Neogene times. *Tectonophysics* **448**, 1–19 (2008).
58. Muirhead, J. D. et al. Evolution of upper crustal faulting assisted by magmatic volatile release during early-stage continental rift development in the East African Rift. *Geosphere* **12**, 1670–1700 (2016).
59. Sherrod, D. R., Magigita, M. M. & Kwelwa, S. *Geologic Map of Oldonyo Lengai (Oldoinyo Lengai) and Surroundings, Arusha Region, United Republic of Tanzania*. Report No. 1306 (U.S. Geological Survey, 2013).
60. Muirhead, J. D., Kattenhorn, S. A. & Le Corvec, N. Varying styles of magmatic strain accommodation in the East African Rift. *Geochem. Geophys. Geosyst.* **16**, 2775–2795 (2015).
61. Bagdasaryan, G., Gerasimovskiy, V. I., Polykov, A. I. & Gukasyan, R. K. Age of volcanic rocks in the rift zones of East Africa. *Geokhimiya* **1**, 84–90 (1973).
62. Mollel, G. F. Petrochemistry and Geochronology of Ngorongoro Volcanic Highland Complex (NVHC) and its Relationship to Laetoli and Olduvai Gorge, Tanzania. PhD thesis, Rutgers Univ. (2007).
63. Burton, M. R., Sawyer, G. M. & Granieri, D. in *Carbon in Earth* (eds. Hazen, R. M. et al.) 323–354 (De Gruyter, 2013).
64. Sano, Y., Tokutake, T. & Takahata, N. Accurate measurement of atmospheric helium isotopes. *Anal. Sci.* **24**, 521–525 (2008).
65. Chiodini, G., Cioni, R., Guidi, M., Raco, B. & Marini, L. Soil CO₂ flux measurements in volcanic and geothermal areas. *Appl. Geochem.* **13**, 543–552 (1998).
66. Chiodini, G. et al. Carbon isotopic composition of soil CO₂ efflux, a powerful method to discriminate different sources feeding soil CO₂ degassing in volcanic-hydrothermal areas. *Earth Planet. Sci. Lett.* **274**, 372–379 (2008).
67. Sinclair, J. A. Selection of thresholds in geochemical data using probability graphs. *J. Geochem. Explor.* **3**, 129–149 (1974).

Acknowledgements This work was funded by the NSF EAR GeoPRISMS Program, grant numbers 1654518 (J.D.M.), 1654433 (T.P.F.) and 1836651 (J.D.), Deutsche Forschungsgemeinschaft (DFG) grant RE 4321/1-1 (M.C.R.) and the Marshall-Heape fund at Tulane University (C.J.E.). We are grateful to COSTECH and Tanzania Wildlife Research Institute for permitting us to conduct research in Tanzania. We thank E. Saria and K. Nkembo for assistance during fieldwork in the Lake Natron region in 2018, G. Kianji for assistance during collection of data in 2014, and K. Rahilly for assisting with field planning.

Author contributions The initial project was conceived by J.D.M., T.P.F., C.J.E. and J.D., with planning and execution of field data collection by J.D.M., T.P.F., C.J.E., A.L., S.J.O., E.K. and M.C.R. CO₂ flux data were compiled and analysed by J.D.M., T.P.F., E.J.J., S.J.O. and A.L., and laboratory analyses of helium and carbon isotopes were performed by T.P.F., H.L., Y.S. and N.T. Compilation and examination of geophysical and gas chemical data were conducted by C.T., J.D.M., C.J.E., J.v.W. and C.A.C. The final model presented in Fig. 4 was conceived and designed by T.P.F., J.D.M., C.J.E., J.v.W., C.A.C. and S.F.F. The manuscript was written by J.D.M. and T.P.F. with contributions from all co-authors.

Competing interests The authors declare no competing interests.

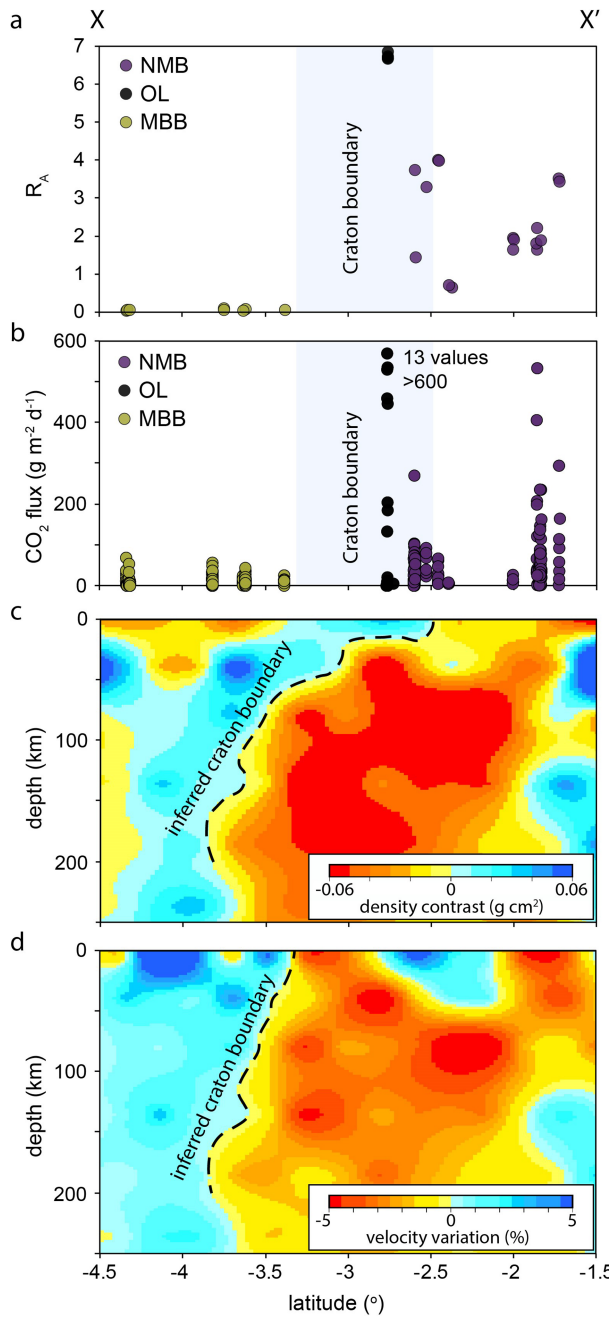
Additional information

Supplementary information is available for this paper at <https://doi.org/10.1038/s41586-020-2328-3>.

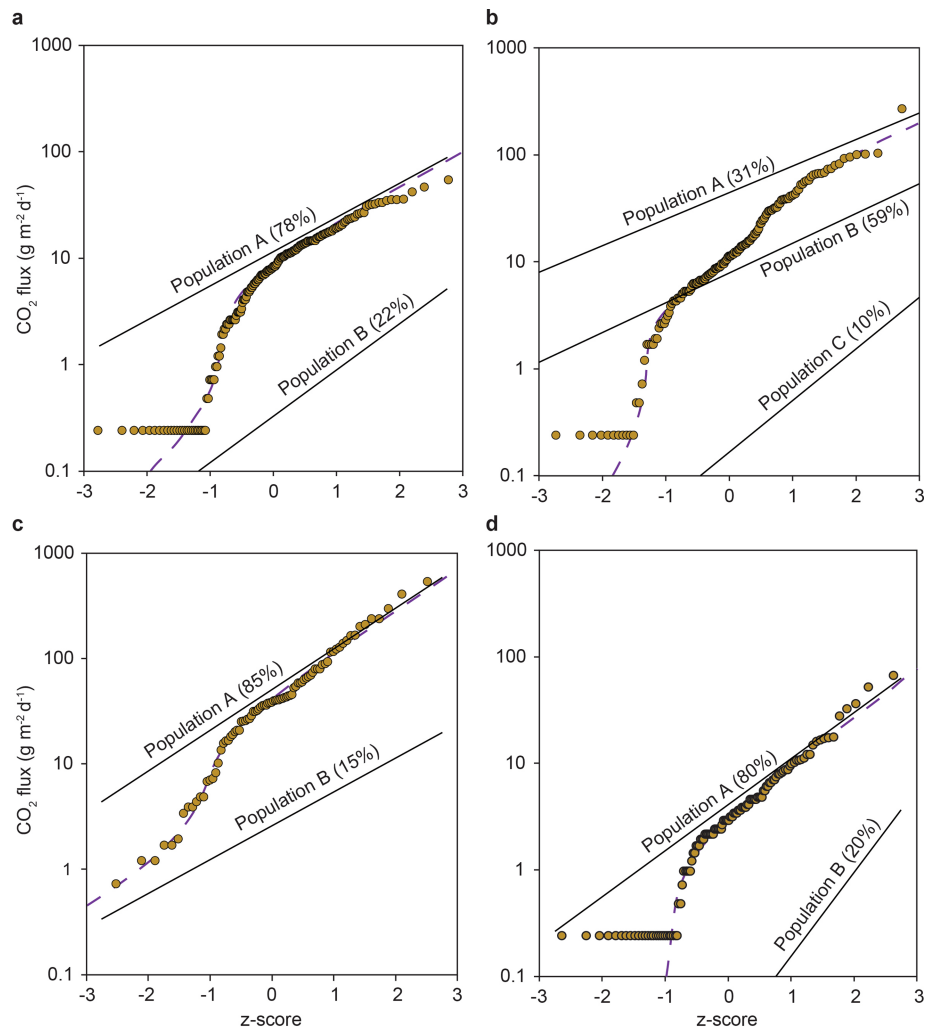
Correspondence and requests for materials should be addressed to J.D.M. or T.P.F.

Peer review information *Nature* thanks Sascha Brune, Giovanni Chiodini and Tanya Furman for their contribution to the peer review of this work.

Reprints and permissions information is available at <http://www.nature.com/reprints>.



Extended Data Fig. 1 | Latitudinal variations in CO₂ flux and R_A values (³He/⁴He) with respect to the modelled lithosphere structure. a. R_A versus latitude along the Eastern Rift from -1.5° to -4.5°. Air-contaminated samples (TZ18-C16) were removed from the analysis. The Tanzanian craton boundary (light grey) is interpreted using the sharp density (c) and velocity (d) contrasts near the northern Manyara and southern Natron basins. It is marked as a broad region to account for location uncertainties and the overall three-dimensional nature of the boundary in the region. **b.** Diffuse CO₂ flux versus latitude along the Eastern Rift from -1.5° to -4.5° for sample sites presented in Fig. 1a and the Oldoinyo Lengai volcano. **c.** Lithosphere density model from Tiberi et al.²¹. **d.** Lithosphere velocity model from Tiberi et al.²¹ (model resolution discussed in Methods). The density and velocity contrasts are relative to the IASP91 model⁴⁹. The position of the cross-section is shown in Fig. 1a.



Extended Data Fig. 2 | CO₂ flux population analyses. a–d, Shown are results for the Manyara (a), Natron (b), Magadi (c) and Balangida (d) basins. The analyses were performed in line with the method of Sinclair⁶⁷ outlined in

Chiodini et al.⁶⁵, with the dashed lines representing a modelled mixed population based on the distributions of the lower, higher and occasionally intermediate flux populations.